Clays and Clay Minerals, Vol. 49, No. 4, 300–309, 2001.

ATOMIC FORCE MICROSCOPY STUDY OF HYDROTHERMAL ILLITE IN IZUMIYAMA POTTERY STONE FROM ARITA, SAGA PREFECTURE, JAPAN

YOSHIHIRO KUWAHARA[1], SEIICHIRO UEHARA[2] AND YOSHIKAZU AOKI[2]

[1]Department of Evolution of Earth Environments, Graduate School of Social and Cultural Studies, Kyushu University, Ropponmatsu, Fukuoka 810-8560, Japan

[2]Department of Earth and Planetary Sciences, Faculty of Science, Kyushu University, Hakozaki, Fukuoka 812-8581, Japan

Abstract—The surface microtopographic observations and analyses of Izumiyama hydrothermal illite particles were made by utilizing tapping-mode atomic force microscopy (TMAFM). The Izumiyama illite particles showed platy to lath shapes. Platy particles exhibited various spiral growth patterns, *i.e.* circular, malformed circular, or polygonal single unit-cell layer spirals, polygonal parallel step spiral, or interlaced spiral patterns. The polygonal parallel step spiral and interlaced spiral patterns are formed by two single unit-cell layers rotated by 180° and 120° arising from a single screw dislocation point, respectively. The spiral patterns indicate that the illite particles have $1M$, $2O$ and $2M_1$ polytypes. Lath-shaped particles show only interlacing patterns supporting the formation of $2M_1$ structures.

Particles showing circular or malformed circular spirals were found to be thinner and to have narrower step separations than particles showing polygonal spirals. Polygonal platy and lath-shaped particles showing interlaced patterns tended to be thicker and to have wider step separations than the other polygonal platy particles.

These results suggest that the Izumiyama illites crystallize as the result of a mechanism involving solution-mediated polytypes and spiral-type transformations of illite. The mechanism involves the Ostwald ripening process, *i.e.* a transformation of the polytype and spiral shape. The sequence of crystallization of the Izumiyama illite is: $1M$ circular spirals → $1M$, $2O$ polygonal spirals → $2M_1$ polygonal spirals occurring during crystal growth and sequentially overgrowing on the initial particle surfaces. The supersaturation of the hydrothermal solution probably decreases gradually during the transformation, and this decrease may cause not only the transformation from a circular to a polygonal crystal morphology but also the development of a lath habit due to the inhibition of the growth rate in the [010] direction of the particle.

Key Words—Atomic Force Microscopy (AFM), Hydrothermal Illite, Microtopography, Morphology, Polytype, Spiral Growth, $2O$ Polytype.

INTRODUCTION

Morphological data can provide information on the type of reaction that last affected a mineral surface (Nagy, 1994). For example, the crystal shapes and sizes of illite particles from sedimentary basins can provide information regarding the rate law for illite growth kinetics in sandstone reservoirs (Nagy, 1994). The morphology of the growth spirals of micas can potentially yield information on the solution saturation state during crystal growth (Blum, 1994; Kitagawa, 1998), and it is very important to obtain an understanding of growth mechanisms and polytypism (Baronnet, 1972; Kuwahara *et al.*, 1998).

After Frank (1949) suggested the spiral-growth mechanism to account for the growth of vapor-phase crystals, growth spirals of unit-cell-order step heights were initially observed on many mineral surfaces by means of phase-contrast and interference-contrast microscopy (Verma, 1956; Sunagawa, 1960, 1961, 1962, 1964; Komatsu and Sunagawa, 1965). These methods are extremely sensitive in vertical resolution, but the lateral resolution is limited to that of optical microscopy (Sunagawa and Koshino, 1975).

The platinum-carbon (Pt-C) replica and gold-decoration methods have been applied to clay minerals (kaolin minerals: Gritsaenko and Samotoin, 1966; Sunagawa and Koshino, 1975; hydrothermal illite: Tomura *et al.*, 1979; Kitagawa *et al.*, 1983; Kitagawa, 1998) and synthetic micas (Baronnet, 1972) to reveal further surface microtopography. The thickness of samples is primarily calculated from the length of their shadows cast at a low angle in Pt-shadowed specimens for transmission electron microscopy (TEM) (Lindgreen *et al.*, 1991). However, the thickness measurement of the shadowed specimens is accurate to ±4 Å at a shadowing angle of 10° (Nadeau *et al.*, 1987), making it difficult to tell whether the thickness is within 10 or 7 Å, *i.e.* a 2:1 or 1:1 layer (Lindgreen *et al.*, 1991, 1992).

Atomic force microscopy (AFM) is a promising tool for quantifying surface microtopography on the order of the unit-cell and can produce surface atomic-resolution images of both conductors and non-conductors. The use of AFM for clay particles permits morphological measurements of high accuracy, including particle dimensions, step heights, and step separations and the determination of many properties of individual particles, that cannot be obtained by other techniques

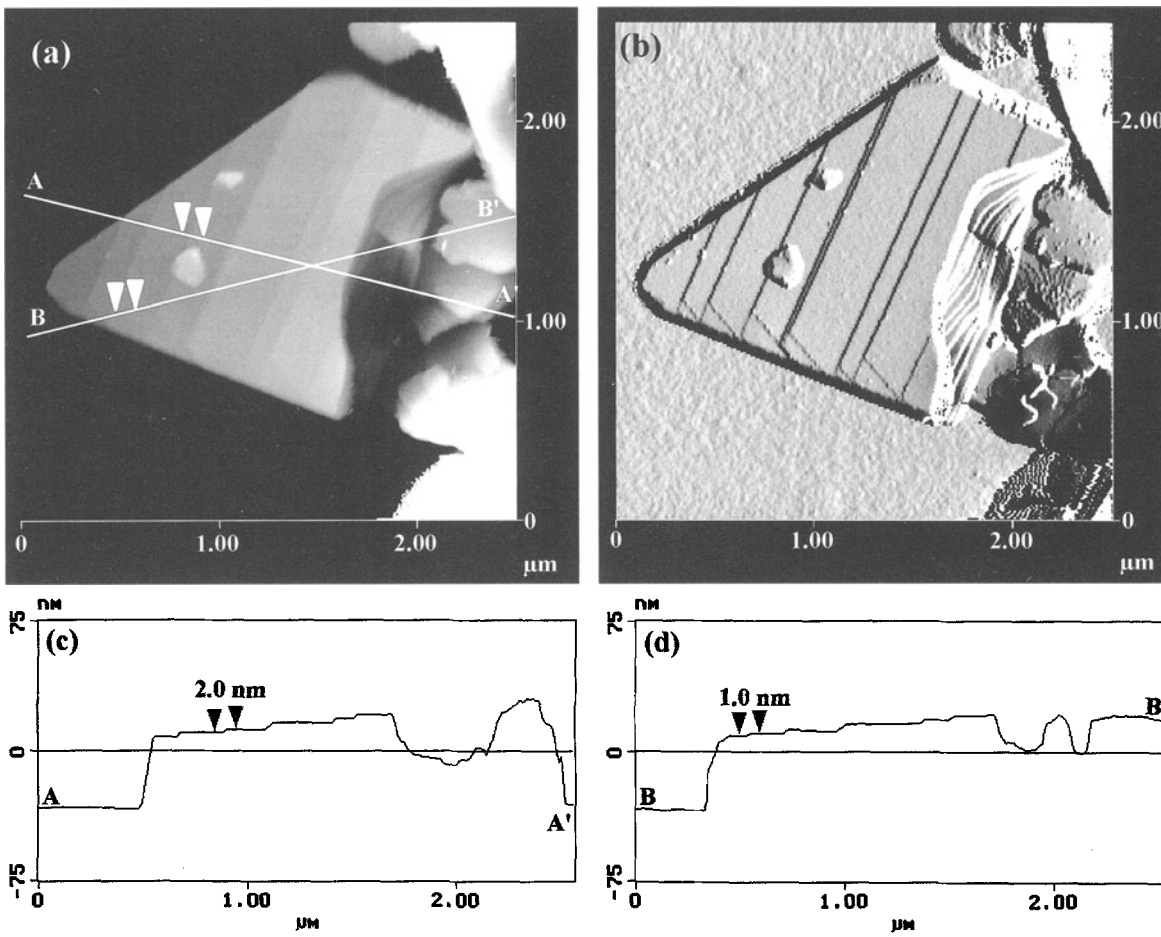

Figure 1. TMAFM height image (z = 150 nm) (a) and amplitude image (b) of an Izumiyama hydrothermal illite particle showing interlacing patterns on the (001) surface. (c) and (d) Cross-sectional views along A–A′ and B–B′ white lines in (a), respectively.

(Lindgreen *et al.*, 1991, 1992; Blum, 1994; Nagy, 1994; Kuwahara *et al.*, 1998).

Polytype transformations from $1M$ to $2M_1$ in illite or muscovite is known to occur with increase in temperature and/or with decrease in the supersaturation of a solution (Velde, 1965; Mukhamit-Galeyev *et al.*, 1985; Inoue *et al.*, 1987, 1988; Baronnet, 1992). In addition, TEM and powder X-ray diffraction (XRD) studies of hydrothermal illite and synthetic mica have suggested that the growth habit depends strongly on the mica polytype, *i.e.* $1M$ laths and $2M_1$ platelets (Inoue *et al.*, 1987, 1988; Baronnet, 1992). Kuwahara *et al.* (1998), however, showed by AFM that many lath-shaped hydrothermal illite particles in the Izumiyama pottery stone from Saga prefecture, Japan, exhibit interlaced spiral patterns on their (001) surfaces, supporting the existence of a $2M_1$ polytype. These results are inconsistent with the previous conclusion regarding the shapes of $1M$ laths and $2M_1$ platelets based on TEM and XRD studies. Therefore, in this study we performed AFM analyses for a variety of particles other than the lath-shaped particles of the Izumiyama hydrothermal illites to clarify the growth mechanism and the relationship between the morphology and polytype of illite.

MATERIALS AND METHODS

Hydrothermal illite, sample IZ-2, (Hirasawa and Uehara, 1999) used in the experiment, was obtained from Izumiyama pottery stone from Arita, Saga prefecture, Japan, and is the same sample as described previously by Kuwahara *et al.* (1998). Sample IZ-2 is a white clayey ore from illite veins of the inner illite zone (Nakagawa *et al.*, 1995) and is nearly pure illite, for which the polytype is a mixture of $1M$ and $2M_1$, based on XRD (Hirasawa and Uehara, 1999). The age and temperature of the hydrothermal alterations related to the formation of the Izumiyama pottery stone deposit are estimated at 2.4–2.3 Ma and ~250°C, respectively (Maeda *et al.*, 1996; Hirasawa and Uehara,

https://doi.org/10.1346/CCMN.2001.0490404 Published online by Cambridge University Press

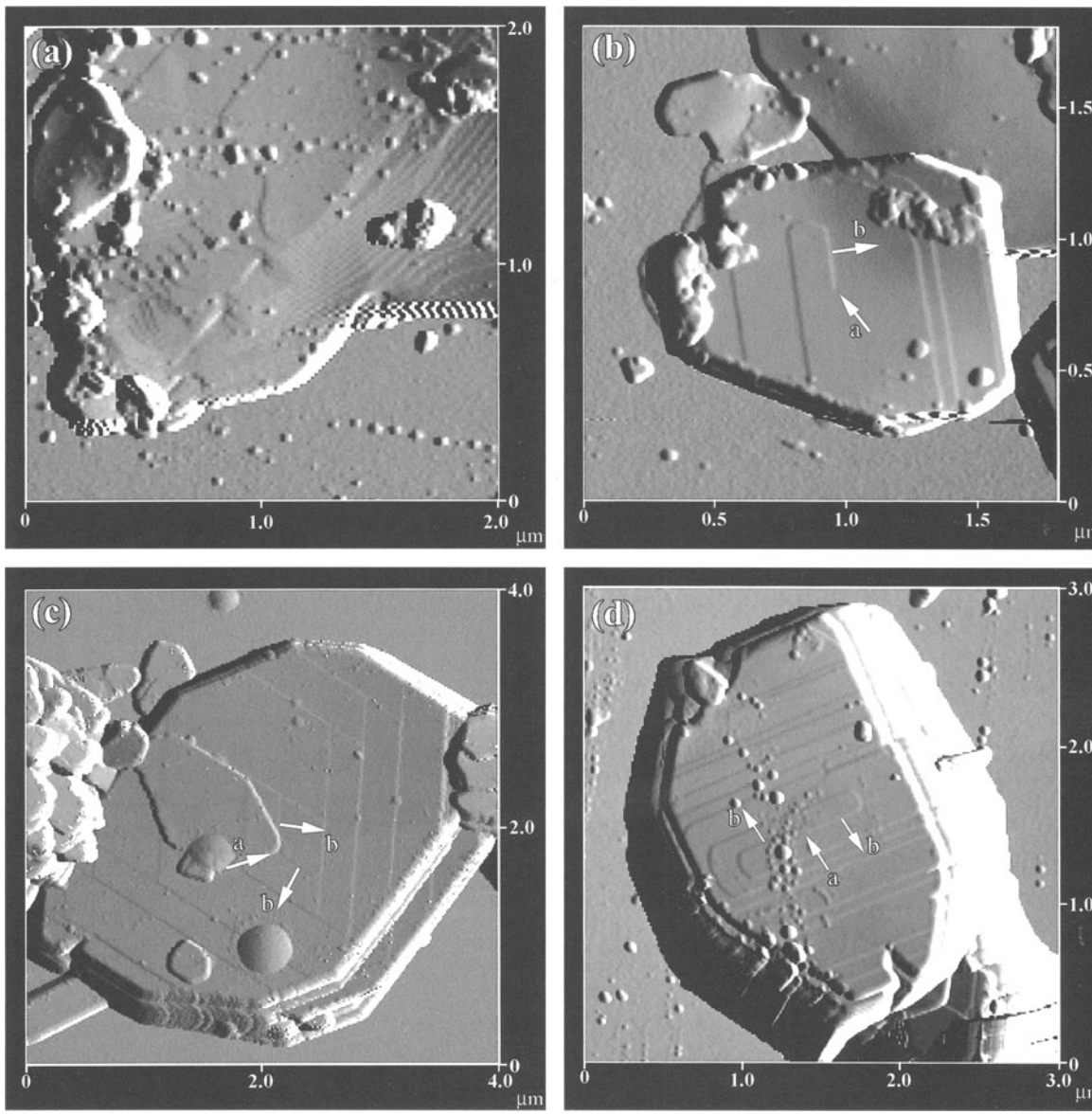

Figure 2. (a) TMAFM amplitude image showing malformed circular spiral patterns on the (001) surface of an illite particle. Each step has a height of 1.0 nm. (b) Amplitude image showing polygonal single unit-cell layer spiral patterns on the (001) surface of a polygonal platy illite particle. Each step has a height of 1.0 nm. White solid arrow a indicates a single screw dislocation point generating a single unit-cell layer and arrow b indicates the spiral direction. (c) Amplitude image showing interlacing patterns on the (001) surface of a polygonal platy illite particle. Step height is 1.0 nm within the zig zag parts and 2.0 nm in the parallel parts. White arrow a indicates a single screw dislocation point generating a 120° rotation of two single unit-cell layers and two arrows b indicate the two spiral directions. (d) Amplitude image showing parallel step spiral patterns on the (001) surface of a polygonal platy illite particle. Each step has a height of 1.0 nm. White arrow a indicates a single screw dislocation point generating a 180° rotation of two single unit-cell layers and the two arrows b indicate the two spiral directions.

1999). Our previous scanning electron microscopy (SEM), XRD and AFM studies of the sample showed that the illite crystals have hexagonal or rectangular platy to lath-shaped forms and are concentrated in <5 μm fractions (Kuwahara *et al.*, 1998; Hirasawa and Uehara, 1999).

The sample preparation for the present AFM observation was identical to that of Kuwahara *et al.* (1998). Briefly, a dilute suspension of illite with distilled water was evaporated on a silicon wafer, which is flat at the subnanometer scale. The AFM was performed with Digital Instruments Nanoscope III using a Multimode

https://doi.org/10.1346/CCMN.2001.0490404 Published online by Cambridge University Press

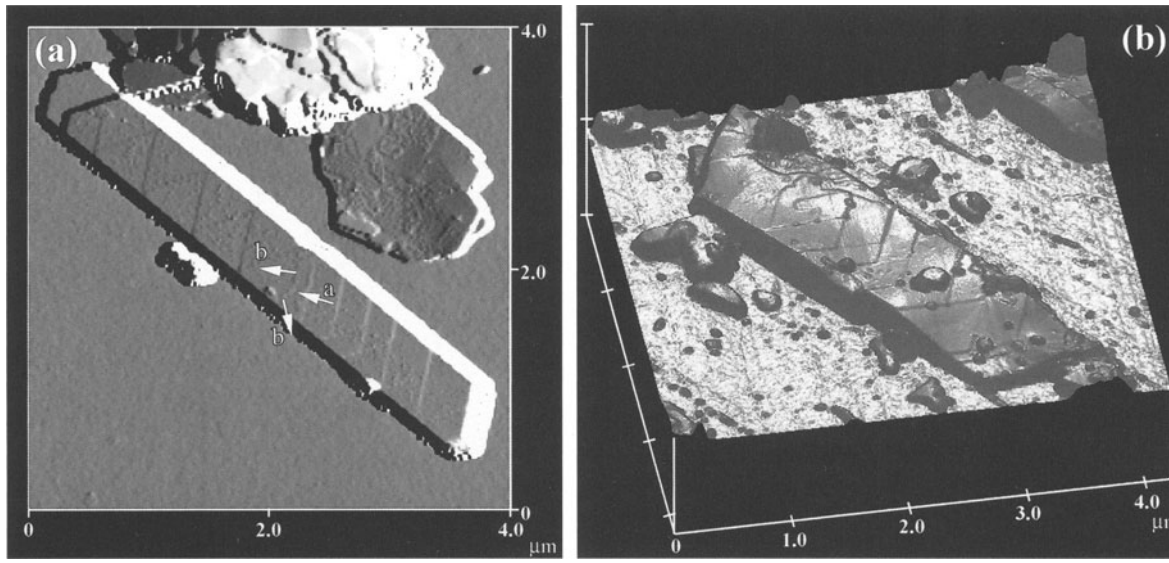

Figure 3. (a) TMAFM amplitude image and (b) illuminated-height image (z = 200 nm) showing interlacing patterns on lath-shaped particle surfaces. Step height is 1.0 nm within the zig zag parts and 2.0 nm within the parallel parts. Lath-shaped particles had euhedral (a) or straight (b) terminations. White arrow a indicates a single screw dislocation point generating a 120° rotation of two single unit-cell layers and two arrows b indicate the two spiral directions.

SPM Head. The samples were scanned in air in tapping mode (TM)AFM, using a J-head piezoelectric scanner (125 μm XY scans and 5 μm Z scan) and 125 μm microfabricated silicon cantilevers. The scanner was calibrated against both an Au-coated proof standard for the X and Y directions (1 μm) and a Pt-coated cross-hatched standard for the Z direction (150 nm). In addition, the c unit-cell height, measured using a mica standard sample (phlogopite), was 1.0 ± 0.08 nm. The scanning frequency was 1.0 Hz.

We collected both parallel height (Figure 1a) and amplitude images (Figure 1b). The height image by TMAFM provides highly accurate height information at ~1.0 nm (Figure 1c, 1d) (Kuwahara *et al.*, 1998). The amplitude image is essentially a record of the error in the height image under a constant force mode, and amplifies the stepped appearance on the surface.

RESULTS

Izumiyama hydrothermal illite particles showed platy (Figure 2) to lath shapes (Figure 3). The individual platy particles are circular, malformed circular, rectangular, hexagonal and other polygonal shapes. They are accompanied by coalesced crystals in some instances. Lath-shaped particles occur as single crystals and have euhedral or straight terminations.

Table 1 shows the morphological data of all Izumiyama hydrothermal illite particles measured by AFM (number of individuals, N, is 162). Table 1 divides the data into three different illite morphologies, *i.e.* circular or malformed circular platy, polygonal platy, and lath-shaped (length/width > 3) particles. The frequencies of the three morphologies are polygonal platy (68%) ≫ lath-shaped ≈ circular or malformed circular platy. The lengths, widths and thicknesses of the polygonal platy particles range from 0.24 to 7.29 μm (mean = 2.16 μm), 0.13 to 5.03 μm (mean = 1.40 μm), and 16 to 591 nm (mean = 113 nm), respectively. The particle dimensions of the circular or malformed circular platy particles are smaller than those of the polygonal platy particles. The lengths and thicknesses of the lath-shaped particles are nearly

Table 1. Morphology and dimensions of all Izumiyama hydrothermal illite particles measured with AFM (N = 162).

Morphology	Circular or malformed circular platy particles	Polygonal platy particles	Lath-shaped particles
Frequency (%)	14	68	18
Length (μm)	0.24–2.93 (1.09 ± 0.004)[1]	0.24–7.29 (2.16 ± 0.005)	0.57–5.97 (3.14 ± 0.005)
Width (μm)	0.22–1.82 (0.76 ± 0.003)	0.13–5.03 (1.40 ± 0.005)	0.16–1.60 (0.65 ± 0.005)
Thickness (nm)	15–66 (31 ± 0.6)	16–591 (113 ± 0.5)	28–438 (122 ± 0.5)
Length/thickness	16.0–59.5 (30.8)	6.8–84.5 (22.2)	12.4–89.7 (31.2)
Width/thickness	12.0–53.0 (22.2)	4.8–59.0 (14.8)	2.4–12.9 (6.3)
Length/width	1.0–2.1 (1.5)	1.0–2.9 (1.6)	3.1–18.5 (5.5)

[1] Figures in parentheses represent the mean value and the error.

https://doi.org/10.1346/CCMN.2001.0490404 Published online by Cambridge University Press

Table 2. Morphology, spiral shapes, and dimensions of Izumiyama hydrothermal illite particles clearly showing spiral patterns on the (001) surface (N = 60).

Morphology and spiral	Circular or malformed circular platy particles (single unit-cell layer circular spiral, 1*M*)	Polygonal platy particles (single unit-cell layer polygonal spiral, 1*M*)	Polygonal platy particles (polygonal spirals of two single unit-cell layers rotated 180°, 2*O*)
Frequency (%)	13	15	10
Length (μm)	0.94–2.93 (1.52 ± 0.004)[1]	1.18–4.67 (2.51 ± 0.004)	0.88–3.82 (2.04 ± 0.005)
Width (μm)	0.85–1.82 (1.15 ± 0.003)	0.94–2.46 (1.37 ± 0.005)	0.56–1.46 (1.12 ± 0.005)
Thickness (nm)	20–66 (42 ± 0.6)	41–184 (98 ± 0.4)	24–218 (93 ± 0.5)
Length/thickness	17.0–59.5 (39.3)	13.3–37.0 (28.0)	10.6–84.3 (33.7)
Width/thickness	17.0–53.0 (31.2)	11.8–33.4 (19.2)	5.2–58.6 (20.4)
Length/width	1.0–1.7 (1.3)	1.1–2.4 (1.5)	1.4–2.6 (1.8)
Mean step separation (nm)	27–56 (44)	74–255 (175)	106–344 (185)

[1] Figures in parentheses represent the mean value and the error.

equal to those of the polygonal platy particles, but the widths of the lath-shaped particles are smaller than those of the polygonal platy particles.

Many of the Izumiyama illite particles show various growth spiral patterns or successive steps on their (001) surfaces. They often exhibit polygonal spirals and in some instances circular or malformed circular spirals. Various types of growth spiral patterns are shown in Figures 2 and 3. The particle dimensions, spiral shapes, and mean step separations of the 60 illite particles with clear spiral patterns within the 162 illite particles in Table 1, are summarized in Table 2. The data are divided into five crystal morphologies and spiral shapes. The frequency distribution of particle thicknesses in the 60 illite particles with clear spiral patterns is nearly equal to that of the particle thicknesses in all of the particles measured by AFM (N = 162). Therefore, the 60 illite particles probably constituted a representative sample for determining the morphological properties of illite particles in the IZ-2 sample.

Figure 2a shows malformed circular spiral patterns on the surface of a malformed platy particle. The step height is 1.0 nm, which corresponds to the thickness of a single 2:1 layer of mica. Illite particles showing such circular spiral patterns, therefore, belong to the 1*M* polytype. The mean particle dimensions and mean step separations of illite particles with circular spiral patterns are the smallest and narrowest, respectively, of the five types (Table 2).

Figure 2b shows a single unit-cell layer polygonal spiral arising from a single screw dislocation point on the surface of a polygonal platy particle. The step height is 1.0 nm, and thus this illite particle belongs to the 1*M* polytype (Baronnet, 1972, 1992; Kuwahara *et al.*, 1998). Figure 2c indicates the interlacing patterns formed by two single unit-cell layers rotated by 120°, originating from a single screw dislocation point on the surface of a polygonal platy particle. The step heights are 2.0 nm in the parallel parts where the front of an advancing step with a single unit-cell height overtakes that of the adjacent lower step and 1.0 nm in the zig zag parts where the one step does not overtake the adjacent lower step. Interlaced spirals and a 120° rotation of two single unit-cell layers confirm that the illite particle belongs to the $2M_1$ polytype (Sunagawa and Koshino, 1975; Kuwahara *et al.*, 1998). The particle thicknesses and mean step separations of the polygonal platy illite $2M_1$ particles are thicker and wider, respectively, than those of the polygonal platy illite 1*M* particles (Table 2). The frequency of polygonal platy particles exhibiting interlacing patterns (42%) is greater than that of the other four types (10–20%).

Figure 2d shows the spiral patterns formed by two single unit-cell layers rotated by 180°, originating from a single screw dislocation point on the surface of a polygonal platy particle. Each step has a height of 1.0 nm, but this crystal exhibits paired step patterns. These findings confirm that the illite particle belongs to the 2*O* polytype. The thicknesses and mean step separations of the illite 2*O* particles are nearly equal to those of the polygonal platy illite 1*M* particles (Table 2). The frequency of illite 2*O* particles in the Izumiyama hydrothermal illites is ~10% (Table 2), although the 2*O* polytype is uncommon in illite or muscovite (Środoń and Eberl, 1984; Griffen, 1992).

Figure 3 shows representative interlacing patterns observed on the (001) surfaces of lath-shaped Izumiyama hydrothermal illite. The interlacing patterns are formed by two single unit-cell layers rotated by 120°, which originates from a single screw dislocation point on the surface (Figure 3a). The step heights are 1.0 nm in the zig zag parts and 2.0 nm in the parallel parts. These lath-shaped particles belong to the $2M_1$ polytype (Kuwahara *et al.*, 1998). The thicknesses of the $2M_1$ lath-shaped particles are nearly equal to those of the polygonal platy illite $2M_1$ particles, whereas the widths and mean step separations of the $2M_1$ lath-shaped particles are narrower and wider, respectively, than those of the polygonal platy illite-$2M_1$ particles (Table 2). No lath-shaped illite particles showing single unit-cell layer polygonal or circular spirals have previously been observed.

Table 2. Extended.

Polygonal platy particles (polygonal spirals of two single unit-cell layers rotated 120°, $2M_1$)	Lath-shaped particles (polygonal spirals of two single unit-cell layers rotated 20°, $2M_1$)
42	20
0.85–5.00 (2.58 ± 0.005)	1.84–5.41 (3.84 ± 0.005)
0.70–2.70 (1.74 ± 0.005)	0.39–1.30 (0.66 ± 0.005)
54–304 (143 ± 0.5)	83–438 (163 ± 0.5)
6.8–50.9 (20.6)	12.4–52.9 (28.2)
4.8–30.6 (14.5)	2.4–12.9 (4.8)
1.0–2.3 (1.5)	3.4–11.3 (6.4)
97–479 (251)	210–797 (436)

DISCUSSION

Spiral-growth and polytype-transformation mechanisms of Izumiyama hydrothermal illites

Our AFM observations clearly show that the Izumiyama hydrothermal illite crystals grew by spiral-growth mechanisms. Many of the Izumiyama illite particles show various spiral-growth patterns or successive single or double unit-cell layer steps on their (001) surfaces. The illite particles having various spiral patterns are divided into five types based on the particle morphology and spiral shape (Table 2). The five types of illite particles have different particle thicknesses, step separations, and polytypes. In addition, the formation of the 2*O* polytype, which is quite uncommon in illite, was first discovered in the present AFM study. These results imply a new illite growth process where the growth rate, spiral growth type, and hydrothermal solution conditions vary during the spiral growth process.

Figure 4 shows the relationship between particle dimension and mean step separations of illite particles divided into five types (Table 2). Platy particles showing circular spirals have the narrowest step separations. Polygonal platy particles showing interlacing patterns tend to have wider step separations than the other platy particles. In other words, illite $2M_1$ particles tend to have wider step separations than illite 1*M* and 2*O* particles. Lath-shaped particles showing interlaced spiral patterns also have wider step separations than illite 1*M* and 2*O* particles.

In general, polygonal (or anisotropic) steps having wider step separations are formed under lower supersaturation conditions than the formation of circular steps with narrower step separations (Sunagawa and Koshino, 1975; Kitagawa *et al.*, 1983; Blum, 1994). The spiral-growth rate of a particle having wider step separations is slower than that of a particle having narrower step separations because of the lower supersaturation conditions (Kuroda, 1984). Therefore, particles having wider step separations should be thinner than those having narrower step separations.

In this study, however, illite particles having wider step separations tend to be thicker than those having narrower step separations (Figure 4c). These results are consistent with a speculative mechanism of solution-mediated polytype transformations for mica based on the Ostwald ripening process (Baronnet, 1980, 1992). According to Baronnet (1980, 1992), during the initial nucleation stage, a large number of $1M_d$ mica particles form. When supersaturation of the solution decreases, the particles smaller than the critical size dissolve to form 1*M* overgrowths on the larger 1 M_d particles. With further decreases in supersaturation, the dissolving, smaller 1*M* particles feed $2M_1$ overgrowths on the larger 1*M* particles.

For the Izumiyama hydrothermal illites, platy illite 1*M* particles having circular spirals were initially formed (probably after the initial stage of Baronnet, 1980, 1992). The smaller particles then dissolved, and 1*M* and/or 2*O* structures with polygonal spirals formed on the (001) surfaces of the larger 1*M* particles having circular spirals. Finally, the $2M_1$ form crystallized on their surfaces. The supersaturation of the hydrothermal solution probably decreased gradually during this transformation.

Blum (1994) estimated the deviation from equilibrium of a solution-precipitated illite particle by measured step separation. The step separation of a spiral (r_{step}) is related to the critical radius of nucleation (r_c), which is defined by the molar volume (V), the surface energy (σ), and the molar free energy of the dissolution reaction (ΔG_{dis}) (Blum and Lasaga, 1987; Blum, 1994),

$$r_{step} \approx 19r_c = 19V\sigma/\Delta G_{dis} \quad (1)$$

The mean values of the step separations of circular single unit-cell layer spirals, polygonal single unit-cell layer spirals, spirals showing a 2*O* structure, interlaced spirals on the platy particle surfaces, and interlaced spirals on the lath-shaped particle surfaces were 44, 175, 185, 251 and 436 nm, respectively (Table 2). Using these mean step separations, V = 140.31 cm^3/mol for muscovite (Robie *et al.*, 1978), and σ = 40.2 ergs/cm^2 for illite (Giese and van Oss, 1993), equation 1 estimates $\Delta G_{dis} \approx$ 2.44, 0.61, 0.58, 0.43 and 0.25 kJ/mol, respectively.

The saturation state of the solution can be estimated from the following equation,

$$\Delta G_{dis} = 2.303RT \log(Q/K) \quad (2)$$

where R is the gas constant, T is temperature, Q is the activity product of the solution, and K is the equilibrium solubility product of illite. A $\log(Q/K)$ value >0 indicates increasing supersaturation and <0 indicates undersaturation. At a formation temperature of 250°C for Izumiyama illite (Maeda *et al.*, 1996; Hirasawa and Uehara, 1999), equation 2 predicts $\log(Q/K)$ = 0.24, 0.06, 0.06, 0.04 and 0.03 for ΔG_{dis} = 2.44, 0.61, 0.58, 0.43 and 0.25 kJ/mol (see above), respectively.

https://doi.org/10.1346/CCMN.2001.0490404 Published online by Cambridge University Press

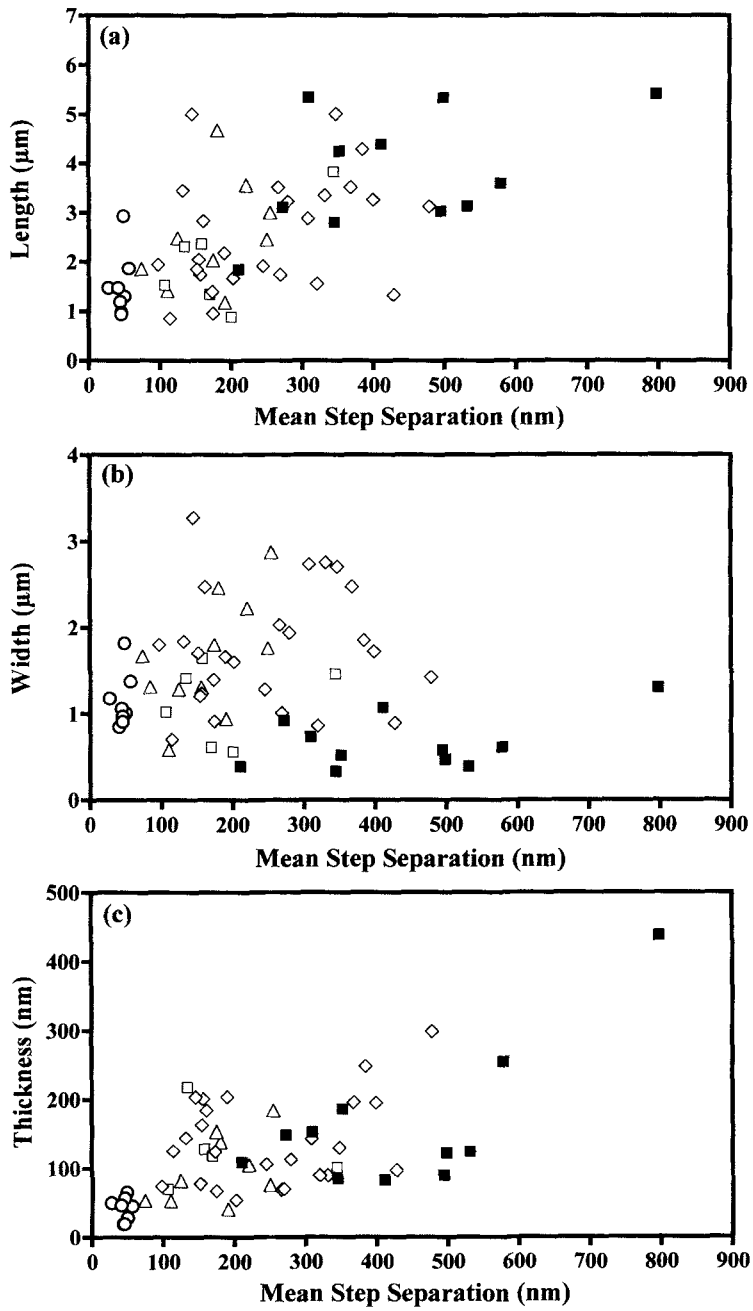

Figure 4. Plots of length *vs.* mean step separation (a), width *vs.* mean step separation (b), and thickness *vs.* mean step separation (c), for individual illite particles showing spiral growth patterns on their surfaces. ○: circular or malformed circular platy particles showing circular or malformed circular spirals, △: polygonal platy particles showing single unit-cell layer polygonal spirals, □: polygonal platy particles showing parallel spiral patterns formed by two single unit-cell layers rotated by 180°, ◇: polygonal platy particles showing interlacing patterns formed by two single unit-cell layers rotated by 120°, ■: lath-shaped particles showing interlacing patterns.

These estimates show that the five types of the Izumiyama illite particles grew under different supersaturation conditions. The particles having 1*M* circular spirals were formed under relatively higher supersaturation conditions. In contrast, the $2M_1$ structures on the platy and lath-shaped particles grew very slowly under solution conditions very close to equilibrium. These results support the suggestion that the supersaturation of the solution forming Izumiyama illites decreased gradually during the polytype transformation

https://doi.org/10.1346/CCMN.2001.0490404 Published online by Cambridge University Press

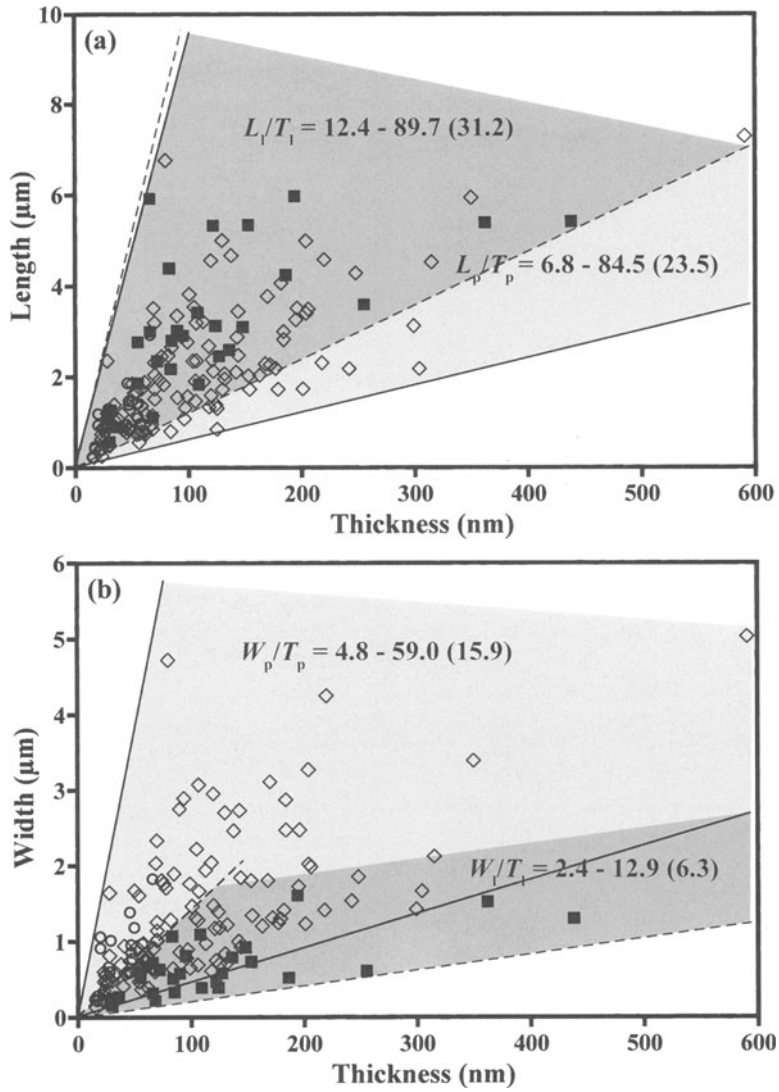

Figure 5. Plots of length *vs.* thickness (a) and width *vs.* thickness (b), for all illite particles measured by AFM. ○: circular or malformed circular platy particles, ◊: polygonal platy particles, ■: lath-shaped particles. L_l/T_l and L_p/T_p represent minimum to maximum values for the ratio of length to the thickness of lath-shaped particles and of platy particles, respectively, and the values in parentheses represent the mean value. W_l/T_l and W_p/T_p represent minimum to maximum values for the ratio of width to the thickness of lath-shaped particles and of platy particles, respectively, and the values in parentheses represent the mean value.

to a spiral shape (1*M* circular spirals → 1*M*, 2*O* polygonal spirals → $2M_1$ polygonal spirals).

The relations between crystal morphology, spiral shape, and polytype in Izumiyama hydrothermal illites

The shape of the growth spirals in the Izumiyama hydrothermal illites was closely related to crystal morphology. The polygonal platy or lath-shaped particles were characterized by polygonal spirals, whereas the circular or malformed circular crystals showed circular or malformed circular spirals. The development of circular or polygonal forms was controlled by the degree of supersaturation of the solution, as described above.

A strong dependence of the growth habit on the polytype of mica, *i.e.* 1*M* laths and $2M_1$ platelets, has been suggested by previous XRD and TEM studies of hydrothermal illites and synthetic micas (Inoue *et al.*, 1987, 1988; Baronnet, 1992). In contrast, our AFM observations of the Izumiyama hydrothermal illites have demonstrated that platy illite particles have 1*M*, 2*O*, $2M_1$ polytypes and lath-shaped particles belonging to the $2M_1$ polytype. The population of 1*M* and 2*O* platy particles in the present study was by no means

https://doi.org/10.1346/CCMN.2001.0490404 Published online by Cambridge University Press

low. These results, however, are inconsistent with previous results.

Figure 5 shows the relationship between the length or width and thickness of Izumiyama illite particles, indicating the relative growth rates of the individual crystal faces. The ratio of length to the thickness of lath-shaped particles (L_l/T_l) was nearly equal to that of platy particles (L_p/T_p). There was also no difference in the degree of lengths or thicknesses between the lath-shaped and platy particles. Therefore, the growth rate in the length direction of the Izumiyama hydrothermal illites was uniform within a certain range, regardless of the crystal morphology. In contrast, the ratio of width to the thickness of the lath-shaped particles (W_l/T_l) is generally smaller than that of the platy particles (W_p/T_p). Specifically, the growth rate in the width direction for the lath-shaped particles was much slower than that for the platy particles.

The elongation of lath-shaped illite has been reported to be parallel to the *a* axis (McHardy *et al.*, 1982; Kantorowicz, 1990; Nagy, 1994), and that the lath-shaped particles in the Izumiyama illites also elongate in the *a* axis direction (Kuwahara *et al.*, 1998). Note, however, that the growth rate in the length direction of the Izumiyama hydrothermal illites is uniform within a certain range, regardless of the crystal morphology, as described above. Hence, the development of the lath-shaped habit was not related to a more rapid growth rate in the [100] direction but related to a much slower growth rate in the [010] (width) direction, relative to the growth rates in the [100] and [010] directions of the platy form, respectively. Specifically, the formation of the lath habit was controlled by the growth rate in the [010] direction of the particles.

It is unclear what controlled the growth rate in the [010] direction of the particles, although the growth rates of individual crystal faces are a function of the surface energy; hence, the growth rates of the (010) faces of illite are lower than those of the (110) prism faces, which are euhedral terminations to the laths and have higher-energy surfaces (Walton, 1967; Nagy, 1994). There is a correlation between the length or thickness and the step separation of the Izumiyama illite particles, regardless of the crystal morphology (Figure 4a, 4c). In contrast, as a function of the width, the step separation was wider in the lath-shaped particles and was narrower in other particles (Figure 4b). In addition, the difference in width between the platy and lath-shaped particles is smaller where the crystals were small and is greater with crystal growth (Figure 5b). Therefore, the decrease of the growth rates of the (010) faces of illite relative to the growth rates of the (110) prism faces may be related to the decrease in supersaturation of the solution as well as to the difference in the surface energy between the (010) and (110) faces.

ACKNOWLEDGMENTS

We thank K. Ishida and Y. Nakamuta of Kyushu University for their helpful suggestions. The authors thank S. Guggenheim of the the University of Illinois at Chicago, G. Henderson of the University of Toronto, and an anonymous reviewer for their helpful and constructive reviews. Y.K. thanks I. Sunagawa of the Yamanashi Institute of Gemmology and Jewellery Arts and M. Nespolo of the National Institute for Research in Inorganic Materials for their fruitful discussions and advice. This study was supported in part by a Research Grant from the Ito Science Foundation and by the Grant-in-Aid for Scientific Research (Y. Kuwahara, No. 137403113) from the Japan Society for the Promotion of Science.

REFERENCES

Baronnet, A. (1972) Growth mechanisms and polytypism in synthetic hydroxyl-bearing phlogopite. *American Mineralogist,* **57,** 1272–1293.

Baronnet, A. (1980) Polytypism in micas: A survey with emphasis on the crystal growth aspect. Pp. 447–548 in: *Current Topics in Material Science, Volume 5* (E. Kaldis, editor). North Hollands, Amsterdam.

Baronnet, A. (1992) Polytypism and stacking disorder. Pp. 231–238 in: *Minerals and Reactions at the Atomic Scale: Transmission Electron Microscopy* (P.R. Buseck, editor). Reviews in Mineralogy, **27.** Mineralogical Society of America, Washington, D.C.

Blum, A.E. (1994) Determination of illite/smectite particle morphology using scanning force microscopy. Pp. 172–202 in: *Scanning Probe Microscopy of Clay Minerals* (K.L. Nagy and A.E. Blum, editors). *CMS Workshop Lectures,* **7.** The Clay Minerals Society, Bloomington, Indiana.

Blum, A.E. and Lasaga, A.C. (1987) Monte Carlo simulations of surface reaction rate laws. Pp. 255–292 in: *Aquatic Surface Chemistry, Chemical Processes at the Particle-Water Interface* (W. Stumm, editor). John Wiley & Sons, New York.

Frank, F.C. (1949) The influence of dislocations on crystal growth. *Discussions of the Faraday Society,* **5,** 48–54.

Giese, R.F. and van Oss, C.J. (1993) The surface thermodynamic properties of silicates and their interactions with biological materials. Pp. 327–346 in: *Health Effects of Mineral Dusts* (G.D. Guthrie and B.T. Mossman, editors). Reviews in Mineralogy, **28.** Mineralogical Society of America, Washington, D.C.

Griffen, D.T. (1992) Micas. Pp. 101–149 in: *Silicate Crystal Chemistry* (D.T. Griffen, editor). Oxford University Press, New York.

Gritsaenko, G.S. and Samotoyin, N.D. (1966) The decoration method applied to the study of clay minerals. Pp. 391–400 in: *Proceedings of the International Clay Conference, Jerusalem, Israel, Volume 3* (L. Heller and A. Weiss, editors). Israel Program for Scientific Translations.

Hirasawa, K. and Uehara, S. (1999) Hydrothermal history of the Izumiyama pottery stone deposit inferred from microtexture and microstructure analysis of illite by SEM and TEM. *Resource Geology,* special issue No. **20,** 113–122.

Inoue, A., Kohyama, N., Kitagawa, R. and Watanabe, T. (1987) Chemical and morphological evidence for the conversion of smectite to illite. *Clays and Clay Minerals,* **35,** 111–120.

Inoue, A., Velde, B., Meunier, A. and Touchard, G. (1988) Mechanism of illite formation during smectite-to-illite conversion in a hydrothermal system. *American Mineralogist,* **73,** 1325–1334.

Kantorowicz, J.D. (1990) The influence of variations in illite morphology on the permeability of Middle Jurassic Brent

Group sandstones, Cormorant Field, UK North Sea. *Marine and Petroleum Geology,* **7,** 66–74.

Kitagawa, R. (1998) Surface microtopography of illite crystals from different modes of occurrence. *Canadian Mineralogist,* **36,** 1559–1567.

Kitagawa, R., Takeno, S. and Sunagawa, I. (1983) Surface microtopographies of sericite crystals formed in different environmental conditions. *Mineralogical Journal,* **11,** 282–296.

Komatsu, H. and Sunagawa, I. (1965) Surface structures of sphalerite crystals. *American Mineralogist,* **50,** 1046–1057.

Kuroda, T. (1984) *Kesshou-ha-ikiteiru (Crystal lives): The Mechanism of its Growth and Transformation of Morphology.* Saiennsu-sha, Tokyo, 256 pp. (in Japanese).

Kuwahara, Y., Uehara, S. and Aoki, Y. (1998) Surface microtopography of lath-shaped hydrothermal illite by Tapping Mode® and Contact Mode AFM. *Clays and Clay Minerals,* **46,** 547–582.

Lindgreen, H., Garnæs, J., Hansen, P.L., Besenbacher, F., Lægsgaard, E., Stensgaard, I., Gould, S.A.C. and Hansma, P.K. (1991) Ultrafine particles of North Sea illite/smectite clay minerals investigated by STM and AFM. *American Mineralogist,* **76,** 1218–1222.

Lindgreen, H., Garnæs, J., Besenbacher, F., Laegsgaard, E. and Stensgaard, I. (1992) Illite-smectite from the North Sea investigated by scanning tunnelling microscopy. *Clay Minerals,* **27,** 331–342.

Maeda, K., Watanabe, K., Izawa, E., Itaya, T. and Takeuchi, K. (1996) K-Ar ages of gold mineralization and argillization in the Arita-Hasami area, western Kyushu, Japan. *Resource Geology,* **46,** 25–31 (in Japanese).

McHardy, W.J., Wilson, M.J. and Tait, J.M. (1982) Electron microscope and X-ray diffraction studies of filamentous illitic clay from sandstones of the Magnus field. *Clay Minerals,* **17,** 23–39.

Mukhamet-Galeyev, A.P., Pokrovskiy, V.A., Zotov, A.V., Ivanov, I.P., and Samotoin, N.D. (1985) Kinetics and mechanism of hydrothermal crystallization of $2M_1$ muscovite: an experimental study. *International Geology Review,* **27,** 1352–1364.

Nadeau, P.H., Wilson, M.J., McHardy, W.J. and Tait, J.M. (1987) Fundamental nature of illite/smectite. *Clays and Clay Minerals,* **35,** 77–79.

Nagy, K.L. (1994) Application of morphological data obtained using scanning force microscopy to quantification of fibrous illite growth rates. Pp. 204–239 in: *Scanning Probe Microscopy of Clay Minerals* (K.L. Nagy and A.E. Blum, editors). *CMS Workshop Lectures,* Volume **7.** The Clay Minerals Society, Bloomington, Indiana.

Nakagawa, M., Nakamoto, J., and Yoshihara, T. (1995) Hydrothermal alteration at the Izumiyama pottery stone deposit, Saga prefecture—Mineralogical properties of quartz and NH_4-bearing sericite. *Journal of Clay Science Society of Japan,* **35,** 1–14 (in Japanese).

Robie, R.A., Hemingway, B.S. and Fisher, J.R. (1978) Thermodynamic properties of minerals and related substances at 298.15 K and 1 bar pressure and higher temperatures. *U.S. Geological Survey Bulletin 1452,* 456 pp.

Środoń, J. and Eberl, D.D. (1984) Illite. Pp. 495–544 in: *Micas* (S.W. Bailey, editor). Reviews in Mineralogy, **13.** Mineralogical Society of America, Washington, D.C.

Sunagawa, I. (1960) Mechanism of crystal growth, etching and twin formation of hematite. *Mineralogical Journal,* **3,** 59–89.

Sunagawa, I. (1961) Step height of spirals on natural hematite crystals. *American Mineralogist,* **46,** 1216–1226.

Sunagawa, I. (1962) Mechanism of growth of hematite. *American Mineralogist,* **47,** 1139–1155.

Sunagawa, I. (1964) Growth spirals on phlogopite crystals. *American Mineralogist,* **49,** 1427–1434.

Sunagawa, I. and Koshino, Y. (1975) Growth spirals on kaolin group minerals. *American Mineralogist,* **60,** 407–412.

Tomura, S., Kitamura, M. and Sunagawa, I. (1979) Surface microtopography of metamorphic white micas. *Physics and Chemistry of Minerals,* **5,** 65–81.

Velde, B. (1965) Experimental determination of muscovite polymorph stabilities. *American Mineralogist,* **50,** 436–449.

Verma, A.R. (1956) A phase contrast microscopic study of the surface structure of blende crystals. *Mineralogical Magazine,* **31,** 136.

Walton, A.G. (1967) *The Formation and Properties of Precipitates, Chemical Analysis, Volume 23.* Interscience Publishers, New York, 232 pp.

E-mail of corresponding author: ykuwa@rc.kyushu-u.ac.jp

(*Received 15 June 2000; revised 3 January 2001; Ms. 460*)